An Analog-Front-End with ultra low-power in optical sensor for FMCW LiDAR system

Yehyeon An
Department of Electronic Engineering
Sogang University
Seoul, Republic of Korea
anyeahan07@sogang.ac.kr

Jonghyun Kim
Department of Electronic Engineering
Sogang University
Seoul, Republic of Korea
yohan623@sogang.ac.kr

Seungju Lee
Department of Electronic Engineering
Sogang University
Seoul, Republic of Korea
wkddk0215@sogang.ac.kr

Jinwook Burm
Department of Electronic Engineering
Sogang University
Seoul, Republic of Korea
burm@sogang.ac.kr

2025 IEEE Asia Pacific Conference on Circuits and Systems (APCCAS) | 979-8-3315-8907-3/25/$31.00 ©2025 IEEE | DOI: 10.1109/APCCAS67402.2025.11376775

***Abstract*—This paper presents an analog front-end (AFE) designed for an optical receiver in a frequency-modulated continuous wave (FMCW) light detection and ranging (LiDAR) system. To achieve high linearity and low noise, a shunt feedback transimpedance amplifier (SF-TIA) is proposed with an input DC current cancellation (IDCC) circuit, followed by a post-amplifier (PA) and a 50 Ω output buffer. The measurement results, implemented in a 28-nm CMOS process with a 1 V supply, demonstrate an AFE gain of approximately 85.5 dBΩ, a bandwidth of 130 MHz, an acceptable input DC current range of 0 µA to 100 µA, an input-referred noise of 4.04 pA/$\sqrt{Hz}$, a power consumption of 343 µW, and chip size of 0.61 × 0.53 mm^2 with I/O pads. Consequently, the overall operation of the optical sensor combined with the transmitter is evaluated to verify system-level performance with a 0.75% accuracy error.**

***Index Terms*—Frequency modulated continuous wave (FMCW) Light detection and ranging (LiDAR), analog front end (AFE), transimpedance amplifier (TIA), input dc current cancellation (IDCC), low power.**

This work is supported by , the MSIT under Grant RS-2025-02653611 (Intelligent Semiconductor Technology Development Program)., Development of Integrated Power System with Embedded GaN Device for Intelligent Muiti-LED Headlamp of Electric Vehicle (RS-2022-00154973), "This research was supported by the MSIT(Ministry of Science and ICT), Korea, under the ITRC(Information Technology Research Center) support program(IITP-2025-RS-2023-00260091) supervised by the IITP(Institute for Information Communications Technology Planning Evaluation)", This work was supported by the Technology Innovation Program (or Industrial Strategic Technology Development Program) (""RS-2023-00235759"", Development of Wireless Charging SoC with Built-In ESD Protection Circuit for Wearable Devices) funded By the Ministry of Trade, Industry Energy(MOTIE, Korea) (1415188115), Korea Institute for Advancement of Technology(KIAT) grant funded by the Korea Government(MOTIE)(P0017011, HRD Program for Industrial Innovation), Brain Korea Four Project., Samsung Electronics Co., Ltd. (IO201221-08244-01), This research was supported by National RD Program through the National Research Foundation of Korea(NRF) funded by Ministry of Science and ICT (RS-2021-NR057239), The chip fabrication was supported by the IC Design Education Center(IDEC), Korea., The EDA tool was supported by the IC Design Education Center(IDEC), Korea., .K-Sensor Development Programs of Korea Planning Evaluation Institute of Industrial Technology (KEIT) grant funded by the Korean Government (MOTIE; grant number: RS-2022–00154782).

I. Introduction

Light Detection and Ranging (LiDAR) systems have rapidly emerged as a promising solution for applications such as autonomous vehicles and 3D imaging technologies [1]. In particular, Frequency-Modulated Continuous Wave (FMCW) LiDAR has several advantages compared to direct Time-of-Flight (dToF) LiDAR. FMCW LiDAR offers high resolution, signal-to-noise ratio (SNR), and measurement of velocity as well as distance and operates with low power for driving the laser diode (LD) by mixing the local oscillator signal with the received signal in the receiver (RX). As a result, the problems indicated in dToF LiDAR, such as eye safety generated by multi-shots consisting of high-power laser pulse signals, are resolved in FMCW LiDAR system [2]. However, the system can generate unwanted DC current due to various factors, resulting in effects of a stable bias condition during signal processing [3]. Furthermore, the detection of useful signal information is limited by the noise level. In this work, an active DC cancellation technique is presented to enhance reliability, and it is designed to minimize noise, area and power consumption for a sensitive and compact LiDAR sensor.

II. System Architecture and Circuit Implementation

A. Frequency Modulated Continuous Wave(FMCW) optical system

FMCW LiDAR system generally measures the round-trip time τ of light and obtains the distance as follows:

$$2R = c * \tau = c * \frac{f_{beat}}{\gamma} \tag{1}$$

where R is the distance to the target, c is the speed of light, γ is the chirp rate (i.e., the slope of the modulated frequency over time), f_{beat} is a beat frequency, meaning the frequency difference between transmitted and received signals.

979-8-3315-8907-3/25/$31.00 ©2025 IEEE
Authorized licensed use limited to: Xi'an Jiaotong-Liverpool University. Downloaded on July 13,2026 at 13:36:10 UTC from IEEE Xplore. Restrictions apply.

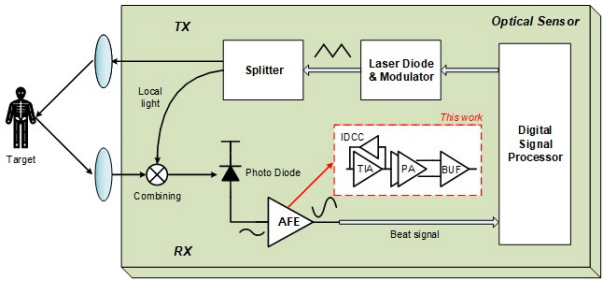

Fig. 1. Overall system architecture of FMCW LiDAR.

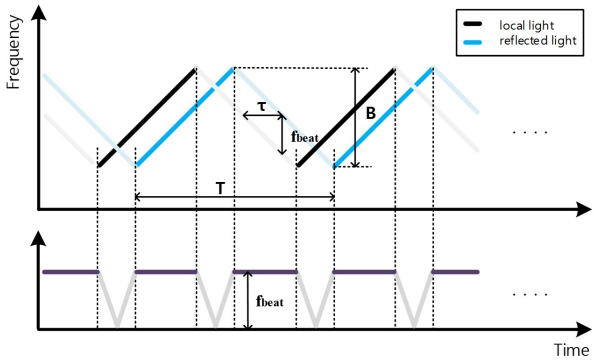

Fig. 2. The process generating the beat signal after combining with local light and reflected light.

In the transmitter (TX) of this system, the LD that generates continuously frequency modulated waveforms (local light) in Fig. 2 is used as a signal source to detect the target. It is important to maintain the linearity of the frequency sweep (i.e., constant γ) because the distortion of the signal occurs if γ varies along the current [2]. As shown in Fig. 1, the laser signal emitted from the TX is reflected by the target, received in the optical sensor, and generates the beat signal combined with local light, where it is converted into current, called the photocurrent, by a photodiode (PD) in the RX. The driving ability of PD is represented by the responsivity [A/W], which indicates how sensitive PD is to light. The current is then amplified and processed by the AFE.

After processing, the measured beat signal that is proportional to distance as described in Equation (1) is synchronized with the reference signal generated in part of the local signal to proceed with the sampling and DSP process [4].

B. Transimpedance Amplifier (TIA)

A transimpedance amplifier (TIA) converts current to voltage, with its gain corresponding to the impedance. Fig. 3(a) shows a simple shunt-feedback transimpedance amplifier (SF-TIA). The transfer function in (2) and the input impedance in (4) are derived as follows:

$$Z_T(s) = -\frac{R_F}{1+sR_F(C_F+C_{IN})}\left(\frac{A_o}{1-A_o}\right) \tag{2}$$

$$\cong -\frac{R_F}{1+sR_F(C_F+C_{IN})} \ (if\ |A_o| \gg 1) \tag{3}$$

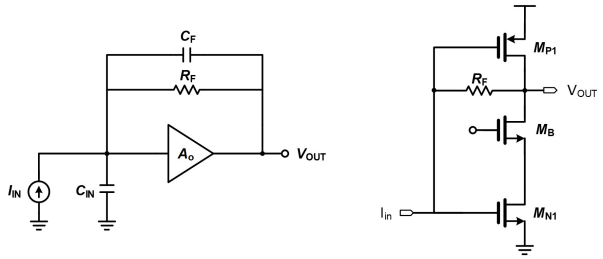

(a) (b)

Fig. 3. (a) Equivalent model of SF-TIA. (b) A proposed SF-TIA.

$$R_{IN}(s) = \frac{V_{IN}(s)}{I_{IN}(s)} = \frac{V_{OUT}(s)}{V_{IN}(s)}\frac{1}{A_o}$$

$$R_{IN}(0) \cong -\frac{R_F}{A_o} \tag{4}$$

$$BW \cong \frac{1}{2\pi R_{IN}C_{IN}} \tag{5}$$

where R_F and C_F are the feedback components, A_o is the open-loop gain, R_{IN} is the input resistance of the TIA, and C_{IN} is the equivalent input capacitance consisting of the PD and I/O pad. Based on this, the bandwidth of the SF-TIA model is approximately given in (5).

The gain of the proposed SF-TIA, shown in Fig. 3(b), is calculated as follows:

$$A_o \cong -(g_{mn1}+g_{mp1})(r_{op1} \parallel g_{mb}r_{ob}r_{on1}) \tag{6}$$

where g_{mn1} and g_{mp1} are the transconductance of M_{N1} and M_{P1}, respectively, and r_{on1}, r_{op1} and r_{ob} are the equivalent small-signal resistance of M_{N1}, M_{P1} and M_B. As shown in (3), A_o should be large enough to approximate R_F as the DC gain. To achieve high gain, the output impedance is boosted by inserting a transistor M_B into the output node.

C. Input DC Current Cancellation (IDCC)

If DC current is generated at the input of the TIA due to several factors, such as the variation in junction bias needed to operate PD in reverse bias or external noise [5], the bias condition of the TIA can be changed, making it impossible to process the signal meaningfully. Therefore, techniques are needed to maintain a stable bias current. In Fig. 4, the circuit for canceling the input DC current is placed between the input and output of the TIA, providing a feedback path by detecting the output voltage of the TIA and feeding the input current of the TIA.

To achieve high gain and low bandwidth in the feedback circuit, the aspect ratio except for M_5 and M_6 is minimized. The overall behavior of the circuit is described by the following:

$$G \cong -\frac{g_{m3}}{1+\frac{g_{m3}R_S}{2}}[(g_{m3}r_{o3}r_{o4}) \parallel (g_{m2}r_{o1}r_{o2})](g_{m5}) \tag{7}$$

$$BW \cong \frac{1}{2\pi[(g_{m3}r_{o3}r_{o4}) \parallel (g_{m2}r_{o1}r_{o2})]C_P(1-A_2)} \tag{8}$$

979-8-3315-8907-3/25/$31.00 ©2025 IEEE
Authorized licensed use limited to: Xi'an Jiaotong-Liverpool University. Downloaded on July 13,2026 at 13:36:10 UTC from IEEE Xplore. Restrictions apply.

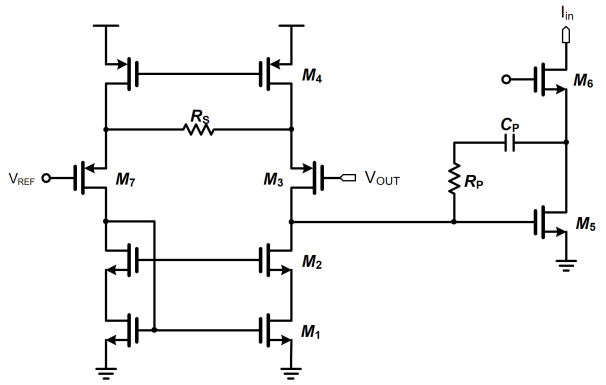

Fig. 4. The feedback circuit for canceling input dc current.

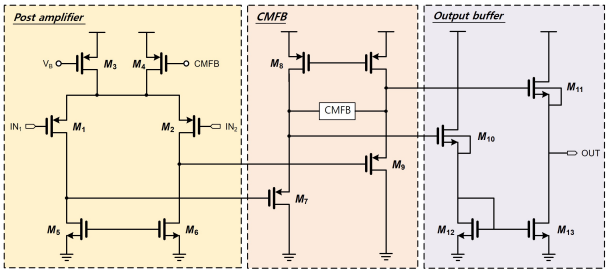

Fig. 5. Other circuits; a fully differential post amplifier and output buffer.

where G and BW are the total gain (voltage to current) and bandwidth for two stages in Fig. 4, A_2 represents the gain of the second stage in (8). By the Miller effect, C_P is multiplied by A_2 at the input node of second stage and R_P, inserted for stability, generates a zero frequency with C_P. Furthermore, the value of the DC current, denoted as I_{in} in Fig. 4, is directly determined by M_5 and M_6, which have to ensure the range of acceptable DC current input.

D. Post amplifier and Output buffer

Figure 5 shows the post-amplifier stage, which boosts the gain for larger output swings. The differential input pair, M_1 and M_2, receives the output voltage from the TIA and the voltage filtered by the low-pass filter (LPF), respectively. The output impedance of the unity gain buffer is designed to be 50 Ω to match the impedance with the measurement setup.

III. Post Layout Simulation Results

Fig. 6(a) shows the total transimpedance gain across the frequency response along the DC in the range of Fig. 6(b) achieved by cascading the stages of TIA, IDCC, PA, and output buffer. Considering the capacitance of the PD and I/O pad in a value of 1.7 pF, the transimpedance gain is 86.8 dBΩ and the bandwidth is from 1.3 kHz to 144.5 MHz when no DC current is injected. The low-frequency cut-off point results from the characteristics of the active feedback loop in the IDCC. In Fig. 7(a), the equivalent noise of the transistors

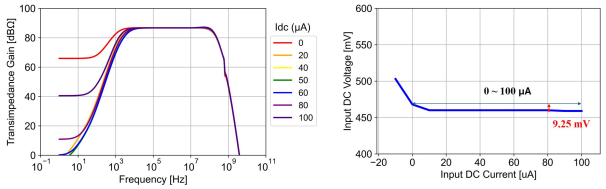

(a) (b)

Fig. 6. (a) Transimpedance gain along the input DC current in range of 0 μA to 100 μA. (b) Input DC cancellation V/I curve for post-simulation results.

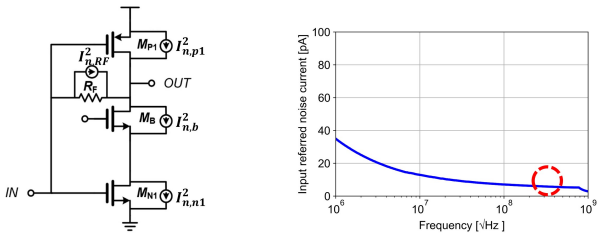

(a) (b)

Fig. 7. (a) Noise analysis of TIA. (b) Frequency response of input referred noise current.

and the resistor is depicted as thermal noise. The average input referred current noise, $\overline{I^2_{n,in}}$ is determined by [6]:

$$\overline{I^2_{n,out}} \cong 4kT\gamma(g_{mp1} + g_{mb} + g_{n1})$$
$$\overline{V^2_{n,out}} = \overline{I^2_{n,out}} Z^2_{out}$$
$$\overline{I^2_{n,in}} \cong \frac{\overline{V^2_{n,out}}}{A^2_o} + \frac{4kT}{R_F} \quad (9)$$

where T and γ are the temperature and the noise figure of the transistor, respectively. For minimizing input noise, as shown in (9), lower transconductance, larger open loop gain and large transimpedance gain are required.

IV. Measurement Results

In Fig. 8, the proposed AFE is implemented in a 28-nm CMOS process with a 1 V supply. By employing the low-voltage threshold (LVT) devices in a fully depleted-silicon on insulator (FD-SOI) technology and incorporating a relatively small number of stages with optimized device sizes, the design achieves significant low power consumption, resulting in a total measured power dissipation of 343 μW.

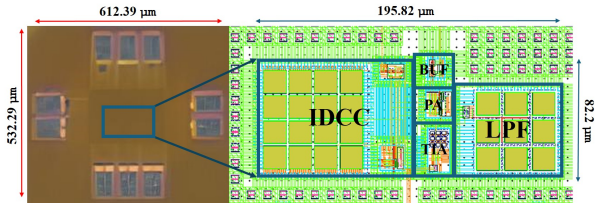

Fig. 8. Micrograph of the proposed AFE circuit.

979-8-3315-8907-3/25/$31.00 ©2025 IEEE
Authorized licensed use limited to: Xi'an Jiaotong-Liverpool University. Downloaded on July 13,2026 at 13:36:10 UTC from IEEE Xplore. Restrictions apply.

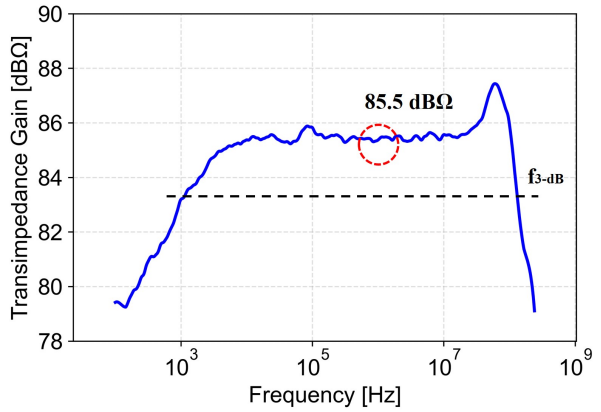

Fig. 9. The measurement of AFE gain and bandwidth at 5 µApp of input current.

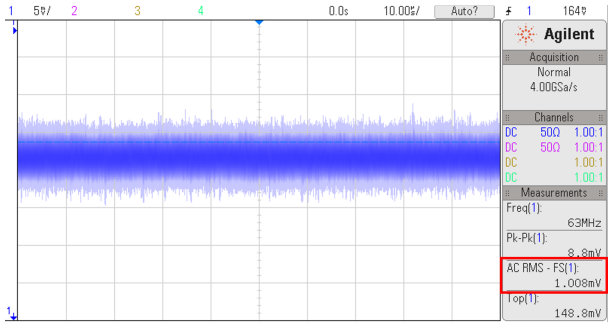

Fig. 10. Output rms noise voltage.

Two methods are conducted to evaluate the performance of the proposed AFE circuit. The frequency response of AFE measured in test mode, and then, an experiment was conducted to evaluate the overall performance and feasibility of the proposed AFE as an optical receiver by implementing overall FMCW LiDAR optical system.

A. *Test mode*

The Tektronix AFG3252 is used to generate the voltage signal, therefore, the series resistor (R_S) is located between the input of the chip and the output of the function generator. In addition, the parallel capacitor (C_{PD}) is implemented in the terminal capacitance of the PIN PD. The value of R_S and C_{PD} is 10 kΩ and 1 pF, which is a typical value specified in the datasheet.

As shown in Fig. 9, the transimpedance gain of 85.5 dBΩ and the bandwidth of 1 kHz to 130 MHz are obtained.

When the AFE input is open-circuited to measure the input-referred noise current, the output RMS noise voltage is measured using the AC RMS Full Screen (standard deviation) function of Agilent Technologies DSO-X 3034A, as shown in Fig. 10, which is also conducted for background noise measurement. Therefore, the input-referred noise of AFE is calculated as follows:

$$\overline{I_{n,in}} = \frac{\sqrt{V_{n,out}^2 - V_{n,background}^2}}{R_f * \sqrt{BW}} \tag{10}$$

TABLE I. PERFORMANCE SUMMARY OF THE PROPOSED AFE WITH PRIOR WORKS

Parameter	[5]	[7]	[8]	This work
Process Technology (nm)	160	180	90	**28**
Architecture	SF-TIA	SF-TIA	SF-TIA	**SF-TIA**
C_{PD} (pF)	2	3	3~15	**1**
Gain (dBΩ)	107	46	60	**85.5**
Bandwidth (MHz)	165	200	450	**130**
Input referred noise (pA/$\sqrt{\text{Hz}}$)	2.29	5	61.3	**4.04**
Input dc current (µA)	-150~250	-125~125	-0.5~0.5V*	**0~100**
Power Consumption (mW)	51.48	119	10.1	**0.343**

*input bias voltage adjustment mechanism.

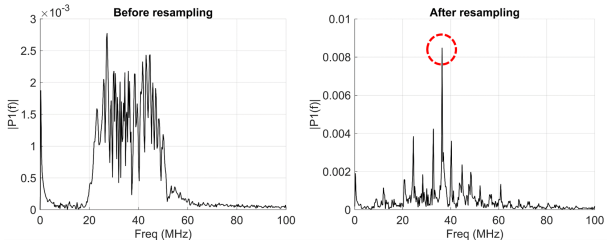

(a) (b)

Fig. 11. Digital signal processing of the beat signal; (a) pre-corrected and (b) post-corrected for target detection.

, resulting in $4.04\ \text{pA}/\sqrt{Hz}$ with 500 µV of background RMS noise. The comparison of other works is given in Table I.

B. *Optical mode*

The overall optical sensor is composed of an off-chip InGaAs PIN photodiode with a responsivity of 0.95 A/W at a wavelength of 1550 nm in RX, combining the LD and the splitter in TX. A triangular wave generated by the function generator is used to drive the LD through an LD controller. There is nonlinear characteristic of LD in the conventional TX system, a linearization resampling technique for highly time-resolved LiDAR was accepted [4]. The comparison between Fig.11 (a), before resampling, and Fig. 11(b), after resampling, shows that the post-corrected FFT result reveals a distinct single-tone frequency.

In this system, a distance of 30 meters was measured, resulting in a measurement error of 0.75% (29.7727 meters). These results validate that the proposed AFE circuit enables high-resolution FMCW LiDAR in dynamic motion.

V. CONCLUSION

The design of the AFE for optical receivers in FMCW LiDAR system using 28 nm CMOS process is presented. The proposed AFE consists of SF-TIA with a feedback loop for input DC cancellation. Two types of measurement results provide the potential to realize low-power and compact solutions for applications such as autonomous vehicles and 3D imaging technologies.

979-8-3315-8907-3/25/$31.00 ©2025 IEEE
Authorized licensed use limited to: Xi'an Jiaotong-Liverpool University. Downloaded on July 13,2026 at 13:36:10 UTC from IEEE Xplore. Restrictions apply.

REFERENCES

[1] B. Behroozpour, P. A. M. Sandborn, M. C. Wu, and B. E. Boser, "Lidar system architectures and circuits," *IEEE Communications Magazine*, vol. 55, no. 10, pp. 135–142, 2017.

[2] B. Behroozpour, P. A. M. Sandborn, N. Quack, T.-J. Seok, Y. Matsui, M. C. Wu, and B. E. Boser, "Electronic-photonic integrated circuit for 3d microimaging," *IEEE Journal of Solid-State Circuits*, vol. 52, no. 1, pp. 161–172, 2017.

[3] Y. Xie, Y. Xin, B. Zhang, R. Yang, Y. Li, and L. Geng, "A wideband and high output swing analog frontend circuit for fmcw lidar," in *2022 IEEE International Conference on Integrated Circuits, Technologies and Applications (ICTA)*, 2022, pp. 172–173.

[4] C. Sun, Z. Chen, S. Ye, J. Lin, W. Shi, B. Li, F. Teng, X. Li, and A. Zhang, "Highly-time-resolved fmcw lidar with synchronously-nonlinearity-corrected acquisition for dynamic locomotion," *Opt. Express*, vol. 31, no. 5, pp. 7774–7788, Feb 2023. [Online]. Available: https://opg.optica.org/oe/abstract.cfm?URI=oe-31-5-7774

[5] X. Zheng, M. Ye, Z. Li, Y. Li, Q. Wang, and Y. Zhao, "A cmos afe array with dc input current cancellation for fmcw lidar," *IEEE Transactions on Very Large Scale Integration (VLSI) Systems*, vol. 32, no. 3, pp. 422–431, 2024.

[6] S. G. Kim, C. Hong, Y. S. Eo, J. Kim, and S. M. Park, "A 40-ghz mirrored-cascode differential transimpedance amplifier in 65-nm cmos," *IEEE Journal of Solid-State Circuits*, vol. 54, no. 5, pp. 1468–1474, 2019.

[7] M. Kashmiri, B. Behroozpour, V. P. Petkov, K. E. Wojciechowski, and C. Lang, "A 4-gs/s 80-db dr current-domain analog frontend for phase-coded pulse-compression direct time-of-flight automotive lidar," *IEEE Journal of Solid-State Circuits*, vol. 55, no. 12, pp. 3131–3145, 2020.

[8] H.-W. Wu, C.-Y. Wang, H.-J. Chen, Y.-C. Lin, P.-H. Hsieh, F.-Y. Lin, Y.-H. Huang, and P.-C. Huang, "A cmos transimpedance amplifier accommodating wide cpd and input bias range for chaos lidar," in *2024 IEEE Asia Pacific Conference on Circuits and Systems (APCCAS)*, 2024, pp. 269–272.

979-8-3315-8907-3/25/$31.00 ©2025 IEEE
Authorized licensed use limited to: Xi'an Jiaotong-Liverpool University. Downloaded on July 13,2026 at 13:36:10 UTC from IEEE Xplore. Restrictions apply.